# Self-Assembled Core–Shell Nanoparticles for Combined Chemotherapy and Photodynamic Therapy of Resistant Head and Neck Cancers

**Chunbai He, Demin Liu, and Wenbin Lin***

Department of Chemistry, University of Chicago, 929 E 57th Street, Chicago, Illinois 60637, United States

**ABSTRACT** Combination therapy enhances anticancer efficacy of both drugs *via* synergistic effects. We report here nanoscale coordination polymer (NCP)-based core–shell nanoparticles carrying high payloads of cisplatin and the photosensitizer pyrolipid, NCP@pyrolipid, for combined chemotherapy and photodynamic therapy (PDT). NCP@pyrolipid releases cisplatin and pyrolipid in a triggered manner to synergistically induce cancer cell apoptosis and necrosis. *In vivo* pharmacokinetic and biodistribution studies in mice show prolonged blood circulation times, low uptake in normal organs, and high tumor accumulation of cisplatin and pyrolipid. Compared to monotherapy, NCP@pyrolipid shows superior potency and efficacy in tumor regression (83% reduction in tumor volume) at low drug doses in the cisplatin-resistant human head and neck cancer SQ20B xenograft murine model. We elucidated the *in vitro/vivo* fate of the lipid layer and its implications on the mechanisms of actions. This study suggests multifunctional NCP core–shell nanoparticles as a versatile and effective drug delivery system for potential translation to the clinic.

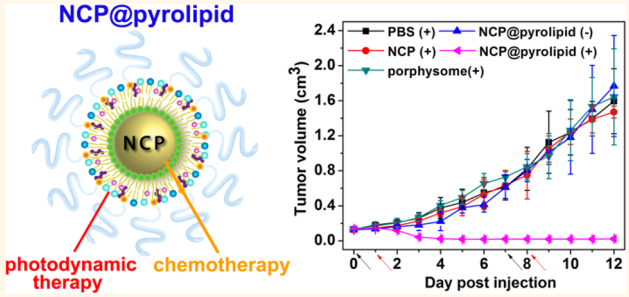


**KEYWORDS:** nanoscale coordination polymer · core–shell nanostructure · combination of chemotherapy and photodynamic therapy · tumor regression

Chemotherapy is a leading treatment for many types and different stages of cancers. However, cancer cells often develop drug resistance and stop responding to chemotherapeutics after repeated sessions of chemotherapy.[1,2] New treatment strategies are needed in order to more effectively eradicate cancer. Combining multiple conventional cancer treatment modalities such as chemotherapy and photodynamic therapy (PDT) can potentially overcome drug resistance through different mechanisms of actions to achieve enhanced anticancer efficacy.[3–5]

PDT is an effective anticancer procedure that involves the administration of a tumor-localizing photosensitizer (PS) followed by light activation to generate highly cytotoxic reactive oxygen species (ROS), particularly singlet oxygen ($^1O_2$), which trigger cell apoptosis and necrosis.[6–9] By localizing both the PS and the light exposure to tumor regions, PDT can selectively kill tumor cells while preserving local tissues.[6,10,11] PDT has been used to successfully treat patients of many different cancers.[12–18] The use of PDT for treating cancers in the head and neck region is particularly advantageous over traditional treatment modalities (*e.g.*, surgery and irradiation) as PDT causes less destruction of surrounding tissues and reduces aesthetic and functional impairments.[19,20] Porphyrin molecules such as Photofrin, Verteporfin, Foscan, Photochlor, and Talaporfin are among the most commonly used PSs for PDT.[11,21,22] Although they have efficient photochemistry for ROS generation, their suboptimal tumor accumulation after systemic administration limits the efficacy of PDT in the clinic.

Nanoparticulate systems can enhance the delivery of small molecule drugs and biologics to tumor sites *via* the enhanced permeability and retention (EPR) effect by taking advantage of leaky blood vasculatures and reduced lymphatic drainage in

* Address correspondence to wenbinlin@uchicago.edu.

Received for review December 6, 2014 and accepted January 5, 2015.

**Published online January 05, 2015**
**10.1021/nn506963h**

tumors.[23−27] Nanoparticles can in principle be used to increase the accumulation of PSs at tumor sites to enhance the PDT efficacy without overly relying on high-precision light delivery.[10,24,28−30] An effective PS nanocarrier must not only have a high payload but also release the agent in a controlled manner to afford a high PS concentration during the typically short duration of light activation (*ca.* 30 min).[31] In addition, the PS agent must have suitable molecular properties to localize inside cancer cells and to minimize self-quenching of their photochemical excited states in order to efficiently generate ROS for selective killing of cancer cells. Because of these stringent requirements, an effective nanocarrier for PDT agents has yet to be developed for clinical use.

We have pioneered the development of nanoscale coordination polymers (NCPs) as a versatile nanoparticle platform for cancer imaging and therapy,[32−43] and recently reported a self-assembled, lipid-coated NCP system for the selective delivery of platinum-based anticancer drugs to a variety of tumors.[32] The NCP core is constructed by linking platinum-based prodrugs with zinc metal ions *via* coordination bonds and then coated with an asymmetric lipid bilayer containing an outer polyethylene glycol (PEG) shell. For example, the NCP particles that carry a cisplatin prodrug have a prolonged blood circulation half-life (~16.4 h) after intravenous injection and the ability to trigger cisplatin release inside cancer cells, leading to enhanced anticancer potency in multiple murine xenograft tumor models.[32] We hypothesize that the NCP particles provide an excellent foundation for constructing multifunctional core−shell hybrid nanoparticles that can selectively deliver and trigger release chemotherapeutic and PDT agents inside cancer cells to enable highly synergistic and effective combination chemotherapy and PDT.

Zheng and Lovell reported the self-assembly of phospholipid-porphyrin (pyrolipid) into porphysomes, a liposome-type of nanoparticles, for PDT in xenograft mouse models.[44−47] In the present study, we construct a novel NCP@pyrolipid core−shell nanoparticle with a cisplatin prodrug in the core and pyrolipid in the shell to enable combination PDT and chemotherapy with a single delivery system. NCP@pyrolipid maintains structural integrity extracellularly but releases cisplatin and pyrolipid in a triggered manner intracellularly to allow for time- and site-specific cytotoxicity. Synergistic actions of chemotherapy from cisplatin and PDT from pyrolipid and light activation by NCP@pyrolipid afford much enhanced anticancer efficacy in head and neck cancer cells and in a xenograft mouse model after intravenous administration when compared to free drugs and monotherapy particles. More importantly, the distinct optical absorption and fluorescence characteristics of pyrolipid and NCP@pyrolipid allow us to elucidate the *in vitro* and *in vivo* fates of the lipid layer of the core−shell nanoparticle and their implications on the mechanisms of actions for combination therapy.

## RESULTS

**Self-Assembly and Characterization of NCP@Pyrolipid.** NCP particles containing a cisplatin prodrug were prepared as previously reported by us.[32] Briefly, a mixture of $Zn(NO_3)_2$ and a cisplatin prodrug, *cis,cis,trans*-[$Pt(NH_3)_2Cl_2$(OCONHP(O)$(OH)_2)_2$], with 1,2-dioleoyl-*sn*-glycero-3-phosphate sodium salt (DOPA) in the Triton X-100/1-hexanol/cyclohexane/water reverse microemulsion was vigorously stirred at room temperature for 30 min to afford spherical DOPA-coated NCP particles of 20 nm in diameter by transmission electron microscopy (TEM, Figure S1, Supporting Information) and 54.1 nm in diameter by dynamic light scattering (DLS, Figure S2). NCP has a cisplatin loading of 25 ± 2 wt % as determined by inductively coupled plasma-mass spectrometry (ICP-MS). NCP was coated with pyrolipid and pegylated to afford NCP@pyrolipid by stirring a tetrahydrofuran (THF) solution (80 μL) of pyrolipid, cholesterol, 1,2-distearoyl-*sn*-glycero-3-phosphocholine (DSPC, pyrolipid/cholesterol/DSPC = 1:1:2 in molar ratios), 20 mol % DSPE-PEG2k, and DOPA-capped NCP in 500 μL of 30% (v/v) ethanol/water at 60 °C for 1 min. The THF and ethanol in the nanoparticle suspension was completely evaporated before subsequent use in *in vitro* and *in vivo* experiments. NCP@pyrolipid contains a self-assembled and asymmetric lipid bilayer, with pyrolipid as a PS for PDT, DSPC as a lipid component to form lipid bilayer, cholesterol as a lipid excipient to order, condense and stabilize the lipid bilayer structure,[48] and DSPE-PEG2k to endow "stealth" and long circulation properties (Figure 1a).[49,50] The NCP cores were synthesized in the presence of DOPA and afforded nanoparticles with a monolayer of DOPA coating *via* Zn-phosphate interactions between NCPs and DOPA molecules and hydrophobic−hydrophobic interactions among DOPA molecules. DOPA-coated NCPs were further coated with DSPC, cholesterol, DSPE-PEG2k, and pyrolipid to yield self-assembled and asymmetric lipid bilayers *via* hydrophobic/hydrophobic interactions between DOPA molecules and the other lipid components.

TEM images of NCP@pyrolipid demonstrated the formation of uniform spherical nanoparticles without aggregation (Figure 1b) and the maintenance of the NCP core structure after lipid coating (Figure S3). DLS measurements gave a Z-average diameter, polydispersity index (PDI), and zeta potential of 108.0 ± 0.2 nm, 0.136 ± 0.012, and −2.3 mV for NCP@pyrolipid dispersed in phosphate buffered saline (PBS), respectively (Figure S4). The small sizes and near neutral surface charge of NCP@pyrolipid suggested their potential in *in vivo* applications. NCP@pyrolipid also exhibited favorable structural stability in physiological environment

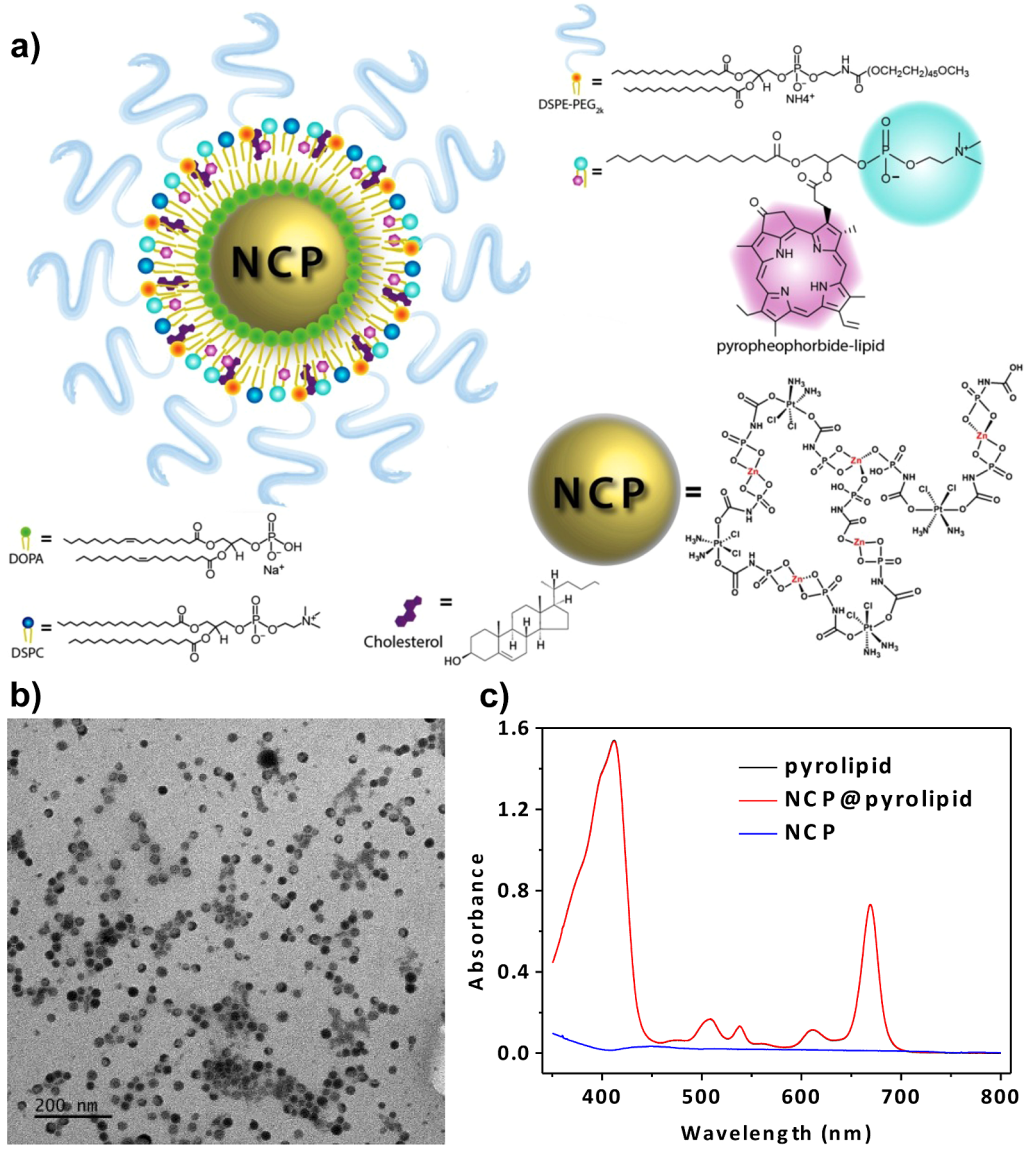


**Figure 1. Schematic illustration, TEM image, and absorption spectra of NCP@pyrolipid. (a) Schematic showing the composition of the self-assembled NCP@pyrolipid core−shell nanoparticle with PEG and pyrolipid in the outer lipid layer. (b) TEM image of NCP@pyrolipid (drop cast from a PBS dispersion). Bar = 200 nm. (c) UV−vis absorption spectra of pyrolipid (black), NCP@pyrolipid (red), and NCP (blue) in THF. The black and red curves overlap completely.**

as evidenced by the unaltered particle size and PDI observed by incubating the particles in PBS containing 5 mg/mL BSA for up to 24 h (Figure S5).

When dissolved in THF or PBS, pyrolipid showed a broad Soret band around 400 nm and a distinct Q-band at 669 nm (Figure 1c and Figure S6). DOPA-capped NCP particles had no absorption at 669 nm (Figure 1c). After lipid coating, NCP@pyrolipid was centrifuged and the pyrolipid amounts in both the supernatant and precipitate were determined by measuring the Q-band absorption at 669 nm. About 265.6 $\mu$g of pyrolipid was coated on the surface of each mg of NCP, corresponding to a pyrolipid to cisplatin weight ratio of ~1:1 (a molar ratio of ~1:3) for NCP@pyrolipid (Figure S7, Table S1). Porphysome was prepared by following the procedure reported by Zheng and co-workers (Figure S8).[44,46]

**Photochemistry.** Pyrolipid was incorporated into the highly oriented and asymmetric lipid bilayer on the surface of NCP@pyrolipid. At sufficiently high pyrolipid loadings, the fluorescence of pyrolipid molecules will self-quench owing to their proximity to each other. Indeed, >96% of the pyrolipid fluorescence of NCP@pyrolipid was quenched when its lipid layer was intact (Figure S9). After addition of Triton X-100, a detergent that can disrupt the lipid bilayer,[44] pyrolipid from the disrupted NCP@pyrolipid regained its fluorescence (Figure S9). As the pyrolipid excited states in intact NCP@pyrolipid are highly quenched, no energy transfer to triplet oxygen was observed, with the generation of negligible amount of $^1O_2$ as determined by the singlet oxygen sensor green (SOSG) reagent (Figure 2a, Figure S10). In contrast, after the disruption

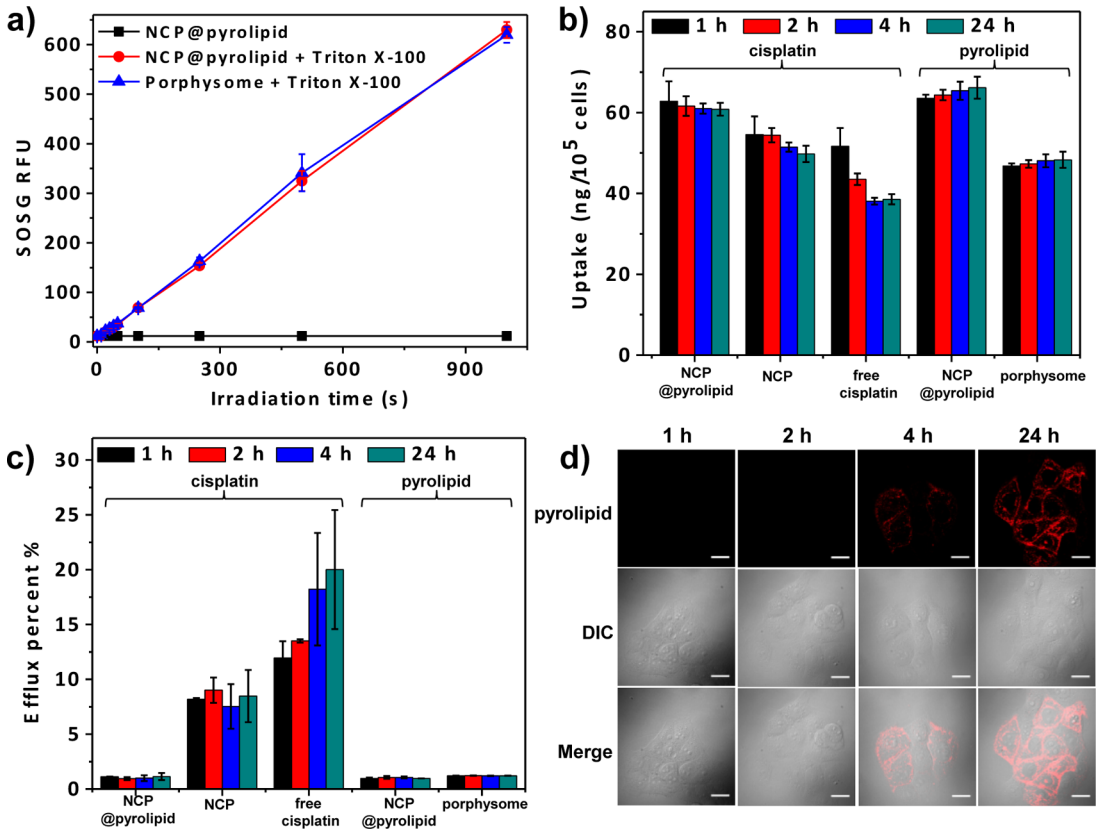


**Figure 2. Singlet oxygen generation and cellular uptake dynamics of NCP@pyrolipid. (a) Time-dependent $^1O_2$ generation by NCP@pyrolipid and porphysome in PBS reported by the SOSG fluorescence intensity (670 nm, 120 mW/cm$^2$) for intact particles *versus* particles with disrupted lipid bilayer. Data expressed as means ± SD ($N$ = 3). (b) Cellular uptake of NCP@pyrolipid, NCP, free cisplatin, and porphysome in SQ20B cells determined by ICP-MS (cisplatin uptake) and fluorimetry (pyrolipid uptake). Data expressed as means ± SD ($N$ = 3). (c) Efflux of cisplatin and pyrolipid of NCP@pyrolipid, NCP, free cisplatin, and porphysome in SQ20B cells. Data expressed as means ± SD ($N$ = 3). (d) CLSM images showing the internalization and intracellular distribution of pyrolipid coated on the NCP in SQ20B cells. Channels are pyrolipid (405 nm laser, red) and DIC. Bar = 20 $\mu$m.**

of lipid layer with Triton X-100, NCP@pyrolipid efficiently generated $^1O_2$ (Figure 2a, Figure S10). The $^1O_2$ generation efficiency of NCP@pyrolipid with disrupted lipid layer was similar to that of porphysome (Figure 2a) after adding Triton X-100 at the same pyrolipid concentration (Figure 2a, Figure S10). Whether the lipid layer is intact or not can therefore be exploited as a "switch" to control the $^1O_2$ generation upon irradiation. It is thus important to understand the stability of the lipid layer of NCP@pyrolipid on its journey to tumor sites after systemic administration and upon entering cancer cells. This understanding will also help us to elucidate the mechanisms of actions for combined PDT and chemotherapy.

**Cellular Uptake Dynamics and Intracellular Lipid Dissociation.** The endocytosis pathway of NCP@pyrolipid was first studied in human head and neck cancer cell SQ20B. The cells were preincubated with a series of uptake inhibitors to block specific internalization pathways, and then incubated with NCP@pyrolipid. The uptake of NCP@pyrolipid significantly decreased in cells treated with $NaN_3$, chloropromazine, genistein, and Me-$\beta$-CD (by 81.2 ± 6.0%, 69.3 ± 1.8%, 59.3 ± 1.7%, and 68.4 ± 1.1%, respectively) but not wortmannin (by 8.4 ± 4.3%), suggesting that the cell uptake is energy-dependent, clathrin/caveolae/lipid raft-mediated endocytosis but not micropinocytosis (Figure S11).[51]

The time-dependent cellular uptake of NCP@pyrolipid was evaluated in SQ20B cells with an incubation time of up to 24 h. Free cisplatin, porphysome, and the original NCP [carrying a cisplatin prodrug and coated with 1,2-dioleoyl-*sn*-glycero-3-phosphocholine (DOPC), cholesterol, and DSPE-PEG2k][32] served as comparisons. As depicted in Figure 2b, the cellular uptake of NCP@pyrolipid was rapid and completed within 1 h, as evidenced by the stable uptake amounts of both cisplatin and pyrolipid over time for up to 24 h. In addition, the uptake amounts of cisplatin and pyrolipid for NCP@pyrolipid were almost identical throughout the 24-h experiment. Considering the weight ratio of pyrolipid to cisplatin in NCP@pyrolipid is ~1:1, we believe that NCP@pyrolipid enters the cells in its intact form. Except for free cisplatin, cellular uptake of cisplatin and pyrolipid remained constant throughout the 24-h experiment. Both cisplatin and pyrolipid uptake amounts of NCP@pyrolipid were higher than those of NCP and porphysome.

In order to understand the cellular uptake dynamics of NCP@pyrolipid, we determined the efflux of cisplatin and pyrolipid in different formulations. SQ20B cells were incubated with NCP@pyrolipid, NCP, free cisplatin, and porphysome for 4 h, and the culture medium was replaced by fresh medium and further incubated for 1, 2, 4, and 24 h. The cisplatin or pyrolipid amounts detected in the culture medium were compared with the 4-h uptake amounts to give the percent efflux (Figure 2c). NCP@pyrolipid showed negligible efflux (<1.5%) of cisplatin and pyrolipid during 24 h incubation. Porphysome showed as low pyrolipid efflux as NCP@pyrolipid. Efflux of free cisplatin increased with time (20.0% at 24 h) and was significantly higher than NCP@pyrolipid and NCP, which results in the decreased cellular cisplatin concentration over time. Efflux of cisplatin for NCP remained at ~8% over time, and was higher than that of NCP@pyrolipid (<1.5%).

Confocal scanning laser microscopy (CLSM) imaging and live cell imaging were also utilized to directly observe the cell internalization and lipid disassociation of NCP@pyrolipid (Figure 2d and Video S1). A 405 nm laser was used for visualizing the pyrolipid. Interestingly, no pyrolipid fluorescence was observed in the first 2-h incubation by CLSM and live cell imaging. The fluorescence appeared after ~2 h of incubation and increased with time. CLSM images also revealed that some of the pyrolipid was incorporated into cell membranes while the rest was distributed in the cytoplasm. As demonstrated earlier, NCP@pyrolipid with intact lipid layer exhibited nearly complete fluorescence quenching. Combining these results, we conclude that NCP@pyrolipid enter the cells in its intact form and maintain structural integrity in the first 2 h followed by the lipid layer dissociation and intracellular lipid redistribution to the cell membrane and cytoplasm. After incorporation into the cell membrane, pyrolipid might change the dynamics, porosity, and permeability of the cell membrane, which could lead to the reduced efflux of both cisplatin and pyrolipid for up to 24 h. This finding indicated that NCP@pyrolipid served as an efficient delivery vehicle for both cisplatin and pyrolipid, making NCP@pyrolipid a promising candidate for combined chemotherapy and PDT.

Time-dependent CLSM imaging results of doubly labeled NCPs (Figure S12) confirmed that NCPs adsorb on the cell membrane and enter the cells as intact core−shell nanostructures as evidenced by the 97.5 ± 5.8% colocalization of the core (red fluorescence coming from Chlorin e6) and shell (green fluorescence from FITC) fluorescence at 10 min. Upon entering the cells, the lipid layers gradually disassociated from the core with the colocalization of red and green fluorescence decreasing to 26.7 ± 4.2% after 1 h and maintaining at the similar level after 2 h (24.1 ± 4.7%). Some green fluorescence from the lipid appeared in the cell membrane while the rest was distributed in the cytoplasm. In contrast, the red fluorescence from the NCP core mostly resided in the cytoplasm.

**Cytotoxicity of NCP@pyrolipid *via* combined chemotherapy and PDT.** Cisplatin causes cytotoxicity mainly by inducing apoptosis while PDT causes cytotoxicity *via* both apoptosis and necrosis pathways.[52,53] By combining chemotherapy and PDT modalities into a single nanoparticle, NCP@pyrolipid can elicit both apoptosis and necrosis efficiently upon irradiation. NCP@pyrolipid is internalized by cells in its intact form and its lipid layer gradually disassociates from the solid core and is translocated to cell membrane or distributed in the cytoplasm. Because of the negligible efflux, cisplatin effectively induces cell apoptosis by binding to DNA whereas pyrolipid accumulates in the cells at a high concentration to efficiently generate $^1O_2$ upon irradiation to cause cell death *via* both apoptosis and necrosis (Figure 3a).

The cytotoxicity of NCP@pyrolipid was evaluated against four human head and neck cancer cells including cisplatin-sensitive HNSCC135 and SCC61 as well as cisplatin-resistant JSQ3 and SQ20B, and was compared with the cytotoxicity induced by free cisplatin (monochemotherapy), NCP (monochemotherapy) and porphysome (mono-PDT). Cisplatin $IC_{50}$ of NCP and free cisplatin showed no significant difference in cells with or without irradiation, indicating that light does not affect the viability of cells treated with formulations without a PS (Table 1, Figure S13−S16). The cytotoxicity of NCP@pyrolipid in cells without irradiation was similar to those of NCP and free cisplatin, and porphysome alone induced no cytotoxicity in cells without irradiation. These results indicate that pyrolipid does not exhibit cytotoxicity without light activation. After irradiation, NCP@pyrolipid exhibited superior cytotoxicity to monochemotherapy (NCP) and mono-PDT (porphysome) as evidenced by its significantly decreased cisplatin and pyrolipid $IC_{50}$ values in all the four cancer cell lines (Table 1, Figure S13−S16). In resistant SQ20B and JSQ3 cell lines, the cisplatin $IC_{50}$ values of NCP@pyrolipid with irradiation decreased by about an order of magnitude when compared to free cisplatin, NCP, and NCP@pyrolipid without irradiation. Upon irradiation, the pyrolipid $IC_{50}$ values of NCP@pyrolipid decreased by 8.0- and 6.2-fold compared with porphysome in SQ20B and JSQ3 cells, respectively. The enhanced cytotoxicity of NCP@pyrolipid upon light activation can be attributed to the synergistic effect of chemotherapy and PDT as evidenced by combination index (CI) values of lower than 1 for SQ20B, JSQ3, and SCC61 cells (Figure S17). These findings were further supported by the flow cytometry results: NCP@pyrolipid with irradiation evoked highest level of apoptosis (26.0%) and necrosis (14.5%) among all of the groups (Figure 3b, Table S2).

***In Vivo* Pharmacokinetic and Biodistribution Studies.** A pharmacokinetic (p*K*) study of NCP@pyrolipid was conducted

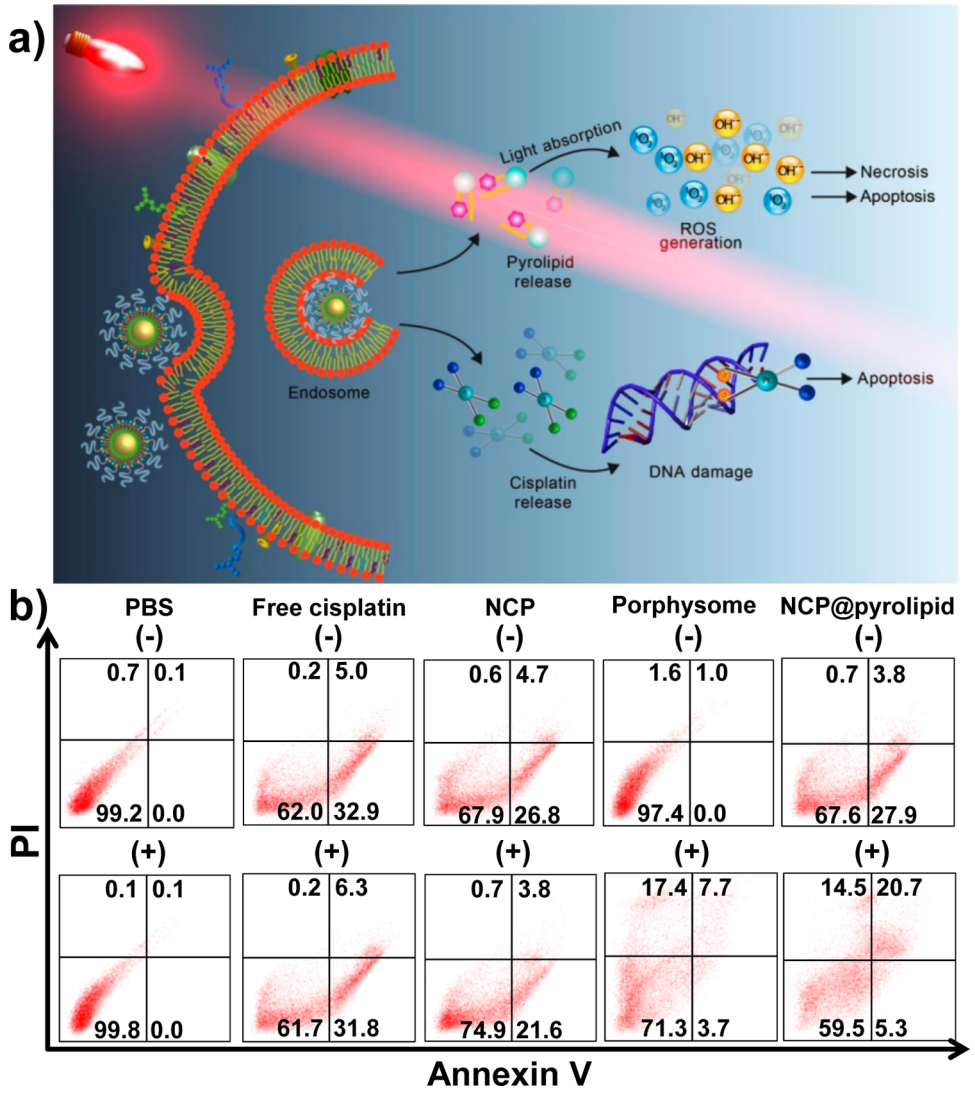


**Figure 3. Proposed cytotoxicity mechanism of NCP@pyrolipid and flow cytometry showing the apoptosis and necrosis induced by NCP@pyrolipid upon irradiation. (a) Schematic showing endocytosis of NCP@pyrolipid and subsequent apoptosis/necrosis achieved by combined chemotherapy and photodynamic therapy. (b) Annexin V/PI analysis of SQ20B cells incubated with PBS (control), free cisplatin, NCP, porphysome, and NCP@pyrolipid with or without irradiation (60 mW/cm$^2$ for 15 min). The quadrants from lower left to upper left (counter clockwise) represent healthy, early apoptotic, late apoptotic, and necrotic cells, respectively. The percentage of cells in each quadrant was shown on the graphs. (+) and (−) refer to with and without irradiation, respectively.**

on CT26 tumor bearing mice to determine the blood circulation time and biodistribution profiles (Figure 4, Figure S18−20, Table S3). The cisplatin distribution was quantified by ICP-MS and the pyrolipid amount in the blood was quantified by UV−vis spectroscopy after extraction by methanol. Both cisplatin and pyrolipid concentrations in blood *versus* time were fitted best by a one-compartment model with nonlinear elimination (Figure 4b,d). The cisplatin and pyrolipid concentrations in blood were similar up to 48 h post intravenous injection, suggesting the lipid bilayer of NCP@pyrolipid remained intact in systemic circulation. Blood circulation half-lives of cisplatin and pyrolipid were determined to be (9.0 ± 1.8) and (6.7 ± 2.2) h, respectively, and did not exhibit statistically significant difference (Figure 4c). In addition to the prolonged blood circulation time, tissue Pt distribution profiles of NCP@pyrolipid showed its ability to avoid uptake by the mononuclear phagocyte system (MPS) as evidenced by the low % ID/g (percent injected dose/gram tissue) in liver (<9.2 ± 0.1%), spleen (<16.7 ± 3.5%), and kidney (<5.6 ± 0.9%, Figure 4a). The slow blood clearance and low MPS uptake led to the high tumor accumulation of drug, with a peak tumor uptake of 23.2 ± 2.4% ID/g 24 h post administration (Figure 4a). The exceptionally high tumor uptake of cisplatin for the NCP@pyrolipid can be partially attributed to the reduced cisplatin efflux due to the incorporation of pyrolipid into cell membranes. We also demonstrated that the slightly different lipid compositions would drastically alter the *in vivo* behaviors of NCP@pyrolipid (Figure S21−S23).

**Antitumor Activity in SQ20B Xenograft Murine Models.** The cisplatin-resistant SQ20B human head and neck cancer

**TABLE 1. Cisplatin and Pyrolipid $IC_{50}$ Values ($\mu$M) in Four Head and Neck Cancer Cell Lines Treated with Various Formulations[a]**

| | irradiation[b] | NCP@pyrolipid | NCP | free cisplatin | porphysome[c] |
|---|---|---|---|---|---|
| HNSCC135 | √ | 1.30 ± 0.05 (0.42 ± 0.02) | 2.71 ± 0.13 | 2.65 ± 0.13 | (0.63 ± 0.02) |
| | × | 3.25 ± 0.46 (1.05 ± 0.15)[d] | 2.71 ± 0.16 | 3.37 ± 0.73 | N/A |
| JSQ3 | √ | 1.21 ± 0.03 (0.39 ± 0.01) | 14.51 ± 1.40 | 13.33 ± 2.03 | (2.42 ± 0.68) |
| | × | 11.39 ± 0.22 (3.67 ± 0.07)[d] | 12.42 ± 0.40 | 11.31 ± 1.20 | N/A |
| SCC61 | √ | 0.77 ± 0.03 (0.25 ± 0.01) | 3.11 ± 0.32 | 3.69 ± 0.28 | (0.50 ± 0.02) |
| | × | 3.48 ± 0.64 (1.12 ± 0.21)[d] | 3.10 ± 0.53 | 3.46 ± 0.08 | N/A |
| SQ20B | √ | 0.41 ± 0.02 (0.13 ± 0.01) | 4.22 ± 0.11 | 4.18 ± 0.11 | (1.04 ± 0.02) |
| | × | 3.97 ± 0.38 (1.28 ± 0.12)[d] | 3.93 ± 0.38 | 3.92 ± 0.15 | N/A |

[a] The numbers in parentheses refer to pyrolipid concentrations. [b] Cells were irradiated with LED light (670 nm) at 60 mW/cm$^2$ for 15 min (equals to 54 J/cm$^2$). [c] Porphysome containing no cisplatin served as controls. The amount of pyrolipid in the porphysome was the same as NCP@pyrolipid under the studied concentrations. [d] The dark cytotoxicity comes entirely from the action of cisplatin in these formulations.

subcutaneous xenograft murine model was employed to assess the *in vivo* antitumor activity of NCP@pyrolipid. All doses were based on free cisplatin or pyrolipid equivalents. SQ20B tumor bearing mice were treated by intravenous injection of (1) PBS, (2) NCP at a cisplatin dose of 0.5 mg/kg, (3) porphysome at a pyrolipid dose of 0.5 mg/kg, or (4) and (5) NCP@pyrolipid at a cisplatin or pyrolipid dose of 0.5 mg/kg once a week for twice. 24 h postinjection, mice in group (1)−(4) were anesthetized with 2% (v/v) isoflurane and tumors were irradiated with a 670 nm LED (100 mW/cm$^2$) for 30 min. As shown in Figure 5, only NCP@pyrolipid plus irradiation showed significant tumor regression in cisplatin resistant SQ20B tumors, with a reduction of tumor volume by ~83%. Mice in the other four groups shared the similar tumor growth pattern, suggesting that monochemotherapy or mono-PDT was incapable of inhibiting tumor growth or regression in the cisplatin-resistant SQ20B tumor model. Mice treated with NCP@pyrolipid but without irradiation (Group 4) showed no tumor growth inhibition, indicating that NCP@pyrolipid achieved anticancer effect in a light-triggered manner. The tumor weight of NCP@pyrolipid with irradiation was ~62-fold smaller than that of control with irradiation group, with a $P$ value of 0.001815 by one-way ANOVA test. We hypothesize that the superior antitumor effect of NCP@pyrolipid upon irradiation is due to the synergistic effect of chemotherapy and PDT. The combination therapy did not cause body weight loss (Figure 5d) or skin damage in the irradiation region (Figure S24), indicating the doses of drug and light are safe to mice.

**Histopathology Analysis, *In Vivo* Apoptosis, and Acute Inflammation.** NCP@pyrolipid exhibited exceptional tumor suppression activity against the cisplatin-resistant human head and neck cancer SQ20B xenograft murine model. A histopathology analysis of resected tumors further confirmed the antitumor potency of NCP@pyrolipid. Tumors of mice treated with NCP@pyrolipid and irradiation showed large areas of apoptosis and necrosis, while mice receiving other treatments had tumors with large regions of viable cancer cells and massive vasculature structures (Figure 6a). PDT eradicates tumors through three main mechanisms: inducing apoptosis/necrosis, activating antitumor immunity against cancers, and disrupting the tumor vasculature structures to deprive the tumor of oxygen and nutrients.[6,11,53] We observed macrophages (smaller nuclei stained with darker blue) infiltration and broken blood vessels in the tumors of mice receiving NCP@pyrolipid and light treatments (Figure 6a). A TUNEL assay was performed on the resected tumors to further substantiate and quantify the *in vivo* apoptosis. As shown in Figure 6b,c, the fluorescence intensity of DNA fragmentation and the relative percentage of apoptotic cells in the NCP@pyrolipid with irradiation were significantly higher than those in the other groups. NCP@pyrolipid with irradiation induced 74.8 ± 4.9% tumor cell apoptosis while the other four groups caused <3.5% apoptosis (Figure 6c). Significant fluorescence coming from dissociated pyrolipid was observed in the tumors of mice treated with NCP@pyrolipid with irradiation at the end point of efficacy study, suggesting the long retention time of pyrolipid in the tumors (Figure S25). Furthermore, no changes in histology were observed for liver, kidneys, lungs, and spleen in mice receiving NCP@pyrolipid and irradiation compared to the control group, suggesting the low toxicity to vital organs (Figure S26).

In order to evaluate the antitumor immunity evoked by the combination of chemotherapy and PDT, mouse blood was collected at the end point and the serum was separated for the determination of TNF-α, IL-6, and IFN-γ production by enzyme-linked immunosorbent assay (ELISA). One of the important mechanisms of the antitumor immunity caused by PDT is the cytokine release and acute inflammation.[53] No significant difference was observed for the three pro-inflammatory cytokine levels among control and monotherapy groups while slightly higher TNF-α ($P$ = 0.047288 *vs* control) and IL-6 ($P$ = 0.031826 *vs* control) were noted for NCP@pyrolipid with irradiation,

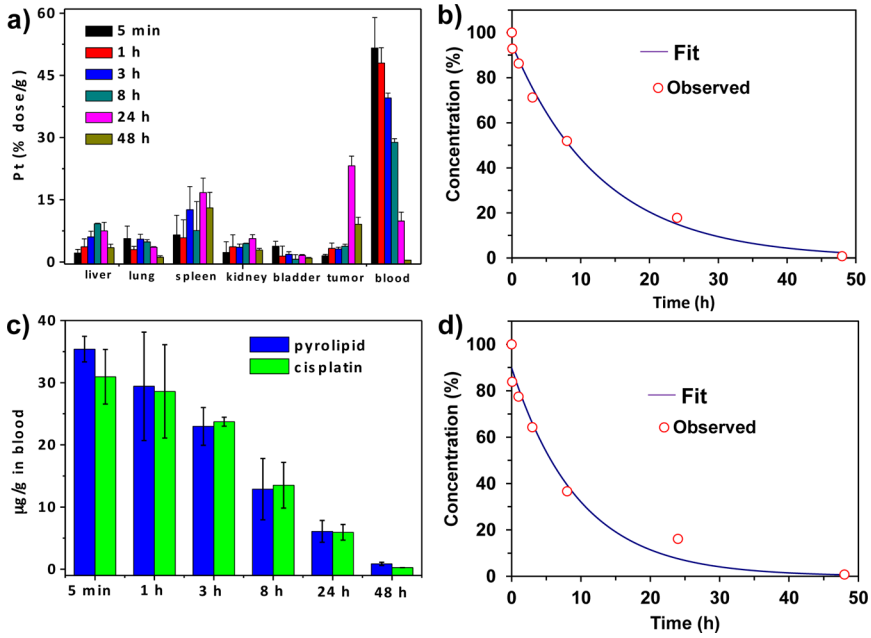


**Figure 4. Pharmacokinetics and tissue distributions of NCP@pyrolipid. (a) Tissue distributions of Pt at time points of 5 min, 1, 3, 8, 24, and 48 h after intravenous injection of NCP@pyrolipid. (b) Observed and fitted time-dependent Pt concentrations in blood following NCP@pyrolipid administration by one-compartment model. (c) Time-dependent pyrolipid and cisplatin concentrations in blood after intravenous injection of NCP@pyrolipid. (d) Observed and fitted time-dependent pyrolipid concentrations in blood following NCP@pyrolipid administration by one-compartment model. Data expressed as means ± SD ($N$ = 3).**

which might be due to the inflammation evoked by PDT (Figure 6d).

## DISCUSSION

Nanotherapeutics achieve high anticancer efficacy with reduced side effects owing to enhanced drug accumulation in tumors.[23,54] The NCPs developed in our lab represent a novel drug delivery platform with high chemotherapeutic loadings, prolonged blood circulation half-lives, and superior anticancer efficacy in multiple murine tumor models.[32] However, after repeated treatments with chemotherapeutic agents, tumor cells develop strategies to increase their resistance to chemotherapy.[55] Combination therapy, such as the combination of chemotherapy and PDT, can promote synergism between different treatment modalities, overcome drug resistance through distinct mechanisms of actions, and enhance the anticancer efficacy.[56,57] To further enhance the potency of the NCP platform, we incorporated the efficient photosensitizer pyrolipid[46] into NCP carrying cisplatin to afford NCP@pyrolipid. We surmised that NCP@pyrolipid can combine the strengths of long blood circulation times and superior chemotherapeutic efficacy of NCP and the potent PDT efficacy of pyrolipid in the same platform to afford maximal anticancer efficacy with low drug doses for the treatment of cisplatin-resistant tumors.

NCP@pyrolipid showed superior anticancer efficacy in cisplatin resistant head and neck cancer over monochemotherapy and mono-PDT. The reasons for the enhanced potency are multifold. First, NCP@pyrolipid provides high loadings of chemotherapeutics and PSs and only releases its cargos in a triggered manner at the site of actions. Second, NCP@pyrolipid possesses prolonged blood circulation time, enhanced cancer cell uptake, and negligible efflux of both chemotherapeutics and PS, allowing for unprecedentedly high delivery efficiency and tumor accumulation. Third, NCP@pyrolipid combines chemotherapy and PDT modalities in one single platform, to synergistically induce apoptosis/necrosis and antitumor immunity in cancers.

NCP@pyrolipid nanoparticles self-assemble into core–shell structures with an asymmetric lipid bilayer coating and carry 25 wt % cisplatin in the core and 25 wt % pyrolipid on the shell, thus showing a remarkable capability of delivering large amounts of both chemotherapeutic agents and PSs. More importantly, NCP@pyrolipid released its payloads in a triggered manner in the site of actions. In the extracellular environment, NCP@pyrolipid maintained its structural integrity. Upon entering cells, the lipid layer gradually dissociated from the solid core of NCP@pyrolipid within 2 h with some pyrolipid fused into cell membrane and the rest remaining in the cytoplasm. After shedding the lipid layer intracellularly, the NCP core became highly permeable to high concentrations of endogenous reducing agents such as cysteine and glutathione to trigger release cisplatin *via* reductive cleavage of the metal–ligand bonds in NCP.[32]

Small molecule drugs typically suffer from nonspecific distribution throughout the body, rapid clearance, and low accumulation at the tumor site when given

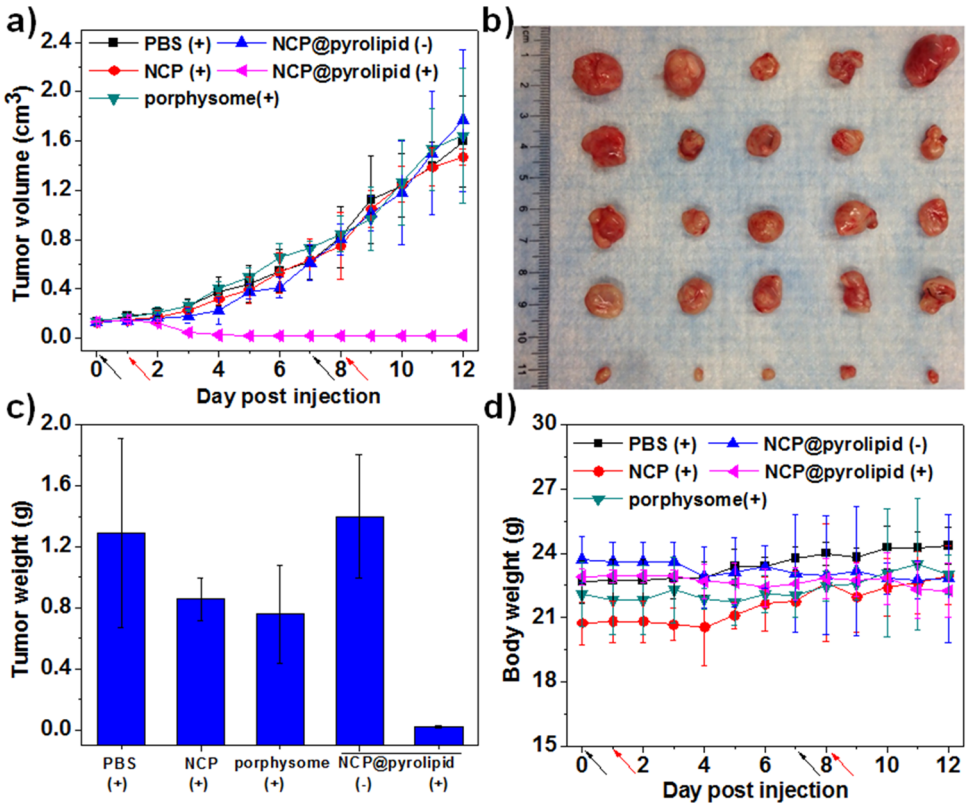


**Figure 5.** *In vivo* **antitumor activity of NCP@pyrolipid. PBS, NCP, porphysome, or NCP@pyrolipid was intravenously injected to human head and neck cancer SQ20B subcutaneous xenograft murine models at a cisplatin dose of 0.5 mg/kg or pyrolipid dose of 0.5 mg/kg followed by irradiation (670 nm, 100 mW/cm$^2$) for 30 min 24 h postinjection. Mice receiving NCP@pyrolipid without irradiation also served as a control. The drug administration and irradiation were performed once a week for twice total. (a) Tumor growth inhibition curve. (b) Photograph of excised tumors on Day 12. From top to bottom: PBS with irradiation, NCP with irradiation, porphysome with irradiation, NCP@pyrolipid without irradiation, NCP@pyrolpid with irradiation. (c) Weights of excised tumors on Day 12. (d) Body weight evolution curve. Data expressed as means ± SD ($N$ = 5). Black and red arrows in (a) and (d) represent the time of drug administration and irradiation, respectively. "+" and "−" in the figure legends refer to with and without irradiation, respectively.**

systemically.[58] Nanoparticles can enhance tumor uptake of drugs *via* the EPR effect.[59] After intravenous injection to tumor bearing mice, NCP@pyrolipid exhibited prolonged blood circulation half-lives for both of its therapeutic payloads: the $t_{1/2}$ values for cisplatin and pyrolipid are (9.0 ± 1.8) h and (6.7 ± 2.2) h, respectively. This excellent p$K$ can be attributed to the small particle size (∼100 nm), high PEG coating (∼20 mol %), and favorable structural stability of NCP@pyrolipid in extracelluar environments. As a result, NCP@pyrolipid achieved as high as 23 ± 2.4 ID%/g cisplatin accumulation in the tumor 24 h post i.v. injection, with low uptake by the MPS system and minimal nonspecific organ distributions.

NCP@pyrolipid not only exhibited efficient and highly specific tumor deposition, but also showed high uptake and accumulation in the cancer cells. The cellular uptake amounts of cisplatin and pyrolipid of NCP@pyrolipid incubated with SQ20B cells were similar and stable over the 24-h experiments. Meanwhile, negligible efflux of cisplatin and pyrolipid was observed for NCP@pyrolipid in SQ20B cells throughout the 24-h incubation peroid. CLSM images also provided evidence that pyrolipid was partly incorporated into the cell membrane and partly retained in the cytoplasm, instead of being recycled out of the cells after disassociation from the solid core of NCP@pyrolipid. The incorporation of pyrolipid into cell membranes could be partly responsible for the negligible cisplatin efflux from cancer cells.

Conventional monochemotherapy often causes drug resistance after cancer patients receive repeated sessions of chemotherapy. Combination therapy offers the opportunities to treat the cancers through different mechanisms of actions, thus leading to enhanced anticancer efficacy *via* synergistic effects.[60] NCP@pyrolipid combined the superior chemotherapy efficacy of cisplatin and potent PDT efficacy of pyrolipid in one single platform and significantly enhanced the anticancer efficacy in cisplatin-resistant head and neck cancer both *in vitro* and *in vivo*. This synergistic effect was substantiated by the following results: (1) significantly decreased cisplatin or pyrolipid $IC_{50}$ values of NCP@pyrolipid with irradiation when compared to free cisplatin, NCP, porphysome with or without irradiation and NCP@pyrolipid without irradiation in the four

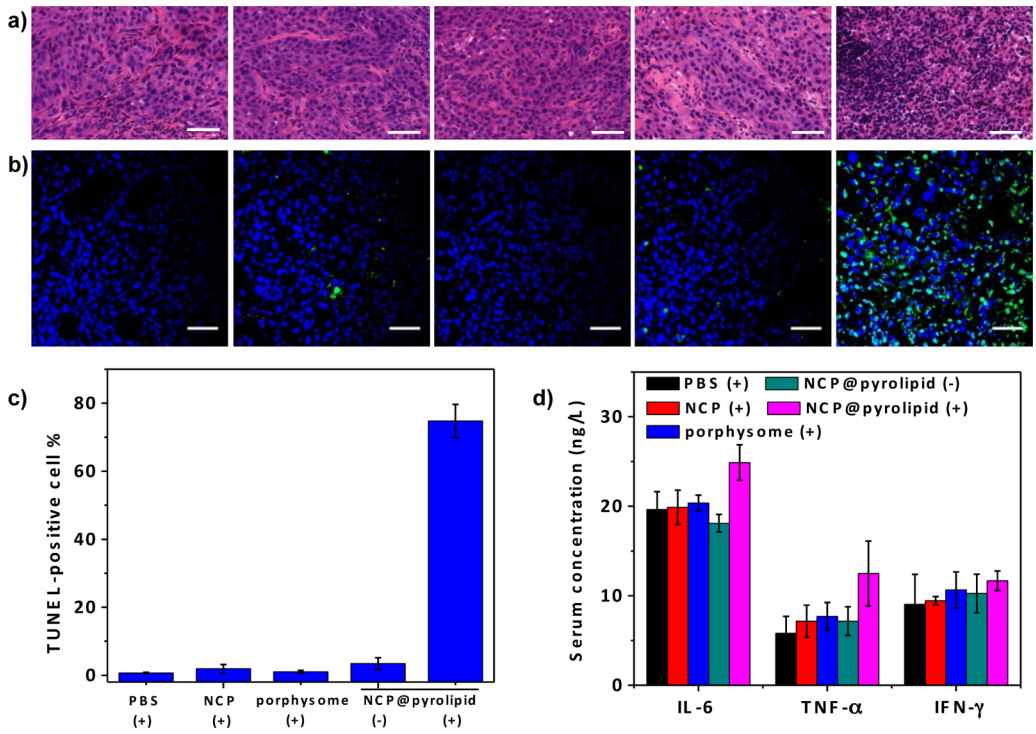


**Figure 6.** *In vivo* **apoptosis and acute inflammation evoked by NCP@pyrolipid. (a) H&E staining of tumor sections harvested from mice receiving PBS with irradiation, NCP with irradiation, porphysome with irradiation, NCP@pyrolipid without irradiation, and NCP@pyrolipid with irradiation (from left to right). Bar = 50 $\mu$m. (b) Representative CLSM images of TUNEL assays of tumor tissues. DNA fragment in apoptotic cells was stained with fluorescein-conjugated deoxynucleotides (green) and the nuclei were stained with DAPI (blue). From left to right: PBS with irradiation, NCP with irradiation, porphysome with irradiation, NCP@pyrolipid without irradiation, and NCP@pyrolipid with irradiation. Bar represented 50 $\mu$m. (c) The percentages of TUNEL-positive cells in tumor tissues. (d) Serum TNF-$\alpha$, IL-6, and IFN-$\gamma$ productions of mice on Day 12. "+" and "−" in the figure legend refer to with irradiation and without irradiation, respectively. Data expressed as means ± SD ($N$ = 3).**

human head and neck cancer cell lines tested; (2) no tumor inhibition was observed for SQ20B tumor bearing mice treated with PBS with irradiation, NCP with irradiation, porphysome with irradiation, and NCP@pyrolipid without irradiation while the tumors of mice receiving NCP@pyrolipid and irradiation shrank by ~83% in volume. Besides apoptosis/necrosis, PDT also induced pro-inflammatory cytokine release and inflammation (Figure 6). Various cell types including malignant cells, tumor endothelial cells, and tumor-infiltrating macrophages have been shown to mediate the acute inflammation after PDT.[61,62] Since we used immunodeficient nude mice as the host for HNSCC xenograft, we were not able to directly evaluate the immune response evoked by PDT. However, this induction of acute inflammation is important in triggering the immune response since it mimics the microbial invasion caused host inflammatory response.[53] We are not aware of literature precedents of significant tumor regression after monotherapy of cisplatin or PDT *via* systemic administration in resistant cancers. We have thus demonstrated for the first time that NCP@pyrolipid shrinks the cisplatin-resistant tumors in mouse xenograft models *via* intravenous administration of nanoparticles carrying both cisplatin and a PS.

Dose limiting side effects prevent complete eradication of most cancers. Untolerably high doses of therapeutics are needed to achieve effective anticancer efficacy owing to the nonideal biodistribution of most drugs.[63] NCP@pyrolipid possesses superior tumor accumulation and minimal nonspecific organ distributions after intravenous injection, thus allowing for enhanced anticancer efficacy with minimal drug doses. We have reported the maximum tolerated dose (MTD) of ≥3 mg/kg in mice for NCP carrying cisplatin.[32] Zheng *et al.* demonstrated that porphysome formed with pyrolipid induced minimal acute toxicity in mice with intravenous doses of 1000 mg/kg.[46] For the present *in vivo* anticancer efficacy study, the mice were intravenously injected with NCP@pyrolipid at a cisplatin dose of 0.5 mg/kg and a pyrolipid dose of 0.5 mg/kg once a week for twice. As indicated by histopathological analysis results, this very low drug dose does not cause *in vivo* toxicity that often occurs for PDT. In comparison, porphysome showed anticancer efficacy only at a pyrolipid dose ≥10 mg/kg in mice[44,46] and the clinical dose of commercially available PSs such as Photofrin is ~3−5 mg/kg in human[64,65] and ~10−12.5 mg/kg in mice.[66,67] Polymeric micelles carrying cisplatin are administrated at a cisplatin dose of 4 mg/kg in mice to inhibit tumor growth.[68] Importantly, the

energy irradiance and irradiation time for PDT were 100 mW/cm$^2$ and 30 min, respectively, with a total light dose of 180 J/cm$^2$, which are comparable to clinical parameters for PDT. This energy irradiance is 1−2 orders of magnitude lower than previous reported PDT by porphysome and gold nanoparticles,[46,69] leading to no skin/tissue damage in the irradiated region. With much lower cisplatin, pyrolipid, and light doses, highly potent antitumor activity was still observed in cisplatin-resistant tumor bearing mice. Through a combination of chemotherapy and PDT, NCP@pyrolipid thus opens a window for achieving maximal anticancer efficacy with minimal drug dose and side effects.

## CONCLUSION

In summary, we have developed a novel NCP-based nanotherapeutic that combines two treatment modalities, chemotherapy and PDT, into one single platform to allow for potent anticancer activity in cisplatin-resistant cancers. NCP@pyrolipid has several distinctive capabilities: (a) carrying exceptionally high loadings of cisplatin and pyrolipid and releasing the payloads in a triggered manner at the site of actions; (b) reducing cisplatin and pyrolipid efflux presumably as a result of cell membrane modification by pyrolipid; (c) effectively avoiding MPS uptake to lead to prolonged systemic circulation after intravenous injection for enhanced and specific tumor accumulation by taking advantage of the EPR effect; (d) combining effective chemotherapy and PDT to exert much enhanced anticancer effect *in vitro* when compared to monotherapy; and (e) achieving significant tumor regression in a cisplatin-resistant tumor model at very low drug doses. The NCP core−shell particles thus offer a general platform for incorporating multiple therapeutic agents or/and modalities for treating many difficult-to-treat cancers, including drug-resistant cancers. As the synthesis of NCPs is highly scalable with little batch-to-batch variations,[32] multifunctional NCPs represent a significant breakthrough in nanomedicine and offer a versatile and effective drug delivery system for potential translation to the clinic.

## METHODS

**Preparation and Characterization of NCP@Pyrolipid.** DOPA-capped NCP nanoparticles were prepared according to our previous report.[32] NCP@pyrolipid was prepared by adding a THF solution (80 $\mu$L) of pyrolipid, cholesterol, DSPC (pyrolipid/cholesterol/DSPC = 1:1:2 in molar ratios), 20 mol % DSPE-PEG2k, and DOPA-coated NCP to 500 $\mu$L of 30% (v/v) ethanol/water at 60 °C. The mixture was stirred at 1700 rpm for 1 min. THF and ethanol were completely evaporated and the NCP@pyrolipid solution was allowed to cool down to room temperature. NCP@pyrolipid was centrifuged at 13 000 rpm for 30 min followed by the removal of the supernatant and resuspending the particles in phosphate buffered solution (PBS).

**Cytotoxicity.** Cytotoxicity of NCP@pyrolipid in head and neck cancer cells. The cytotoxicity of NCP@pyrolipid was tested in four head and neck cancer cell lines including cisplatin-resistant SQ20B and JSQ3 cells and cisplatin-sensitive HNSCC135 and SCC61 cells. The cells were seeded on 96-well plates at 2500 cells/well. After incubating for 24 h, the cells were treated with NCP@pyrolipid, porphysome, NCP, and free cisplatin at various cisplatin concentrations or pyrolipid concentrations. After 24-h incubation, the cells were irradiated with LED light (670 nm) at 60 mW/cm$^2$ for 15 min (equals to 54 J/cm$^2$). The cells without irradiation treatment served as controls. The cells were further incubated for 48 h. The cell viability was detected by (3-(4,5-dimethylthiazol-2-yl)-5-(3-carboxymethoxyphenyl)-2-(4-sulfophenyl)-2*H*-tetrazolium) (MTS) assay (Promega, USA) and the $IC_{50}$ values were calculated accordingly.

**Pharmacokinetics and Tissue Distributions.** Mice were subcutaneously injected in the right flank with 1 million CT26 cells and tumors were allowed to grow until 100 mm$^3$ before they received intravenous administration of NCP@pyrolipid at a cisplatin dose of 3 mg/kg. Animals were sacrificed (3 per time-point) at 5 min, 1, 3, 8, 24, and 48 h after drug administration. After collecting the blood, liver, lung, spleen, kidney, and bladder were harvested. Organs and blood were digested in concentrated nitric acid for 24 h, and the Pt concentrations were analyzed by ICP-MS. The pyrolipid amounts in the blood collected at 5 min, 1, 3, 8, 24, and 48 h were determined using the same extraction and detection method as the recovery experiment (described in Supporting Information). Briefly, the blood was centrifuged at 3,000 rpm for 10 min to separate plasma. Methanol and 0.25% Triton X-100 was added to the plasma for extracting the pyrolipid and preventing aggregation, respectively. The pyrolipid concentrations were determined by UV−vis.

***In Vivo* Anticancer Efficacy.** The PDT efficacy of NCP@pyrolipid was investigated using the SQ20B subcutaneous xenograft murine model. Tumor bearing mice were established by subcutaneous inoculation of SQ20B cell suspension ($5 \times 10^6$ cells per mouse) into the right flank region of 6-week athymic female nude mice. Five groups were included for comparison: PBS with irradiation as control; NCP with irradiation; porphysome with irradiation; NCP@pyrolipid with irradiation; NCP@pyrolpid without irradiation. When tumors reached 100 mm$^3$, NCP, NCP@pyrolipid, and porphysome were i.v. injected to animals at a cisplatin dose of 0.5 mg/kg (corresponding to a pyrolipid dose of 0.5 mg/kg). At 24 h postinjection, mice were anesthetized with 2% (v/v) isoflurane and tumors were irradiated with a 670 nm LED for 30 min. The energy irradiance was measured to be 100 mW/cm$^2$, and the total light dose was 180 J/cm$^2$. Both injection and PDT were performed once a week for twice total. To evaluate the therapeutic efficacy, tumor growth and body weight evolution were monitored. The tumor size was measured with a digital caliper every day. Tumor volumes were calculated as follows: (width$^2$ × length)/2. All mice were sacrificed on Day 12, and the excised tumors were photographed and weighed. The tumors were embedded in optimal cutting temperature (OCT) medium, sectioned at 5-$\mu$m thickness, and subjected to hematoxylin and eosin (H&E) stain for histopathological analysis and TdT-mediated dUTP nick end labeling (TUNEL, Invitrogen, USA) assay for quantifying the *in vivo* apoptosis. The frozen tumor tissue slices were also observed under CLSM using a 405 nm laser to visualize the tumor uptake of NCP@pyrolipid. Liver, lungs, spleen, and kidneys were also excised after the mice were sacrificed, and then embedded in OCT medium, sectioned at 5-$\mu$m thicknes, stained with H&E, and observed for toxicity with light microscopy (Pannoramic Scan Whole Slide Scanner, PerkinElmer, USA). Blood was collected at the end point, and the serum TNF-$\alpha$, IFN-$\gamma$, and IL-6 production was determined by ELISA (R&D Systems, USA).

*Conflict of Interest:* The authors declare no competing financial interest.

*Acknowledgment.* We acknowledge National Cancer Institute (U01−CA151455) for funding support. We thank

Mr. Christopher Poon and Mr. Carter W. Abney for the assistance in ICP-MS analysis. We also thank Dr. Vytas Bindokas and Ms. Shirley Bond for the help with microscopy experiments. C.H., D.L., and W.L. designed the experiments and analyzed the data; C.H. and D.L. conducted the experiments; C.H. and W.L. wrote the manuscript.

*Supporting Information Available:* Detailed methods and additional results (26 figures, 3 tables, and 1 video) on the synthesis and characterization of NCP@pyrolipid and porphysome, singlet oxygen generation, cellular uptake, live cell imaging, CLSM studies, flow cytometry, and pharmacokinetics and tissue distribution. This material is available free of charge *via* the Internet at http://pubs.acs.org.

## REFERENCES AND NOTES


1. Kuczynski, E. A.; Sargent, D. J.; Grothey, A.; Kerbel, R. S. Drug Rechallenge and Treatment beyond Progression-implications for Drug Resistance. *Nat. Rev. Clin. Oncol.* **2013**, *10*, 571–587.
2. Holohan, C.; Van Schaeybroeck, S.; Longley, D. B.; Johnston, P. G. Cancer Drug Resistance: an Evolving Paradigm. *Nat. Rev. Cancer* **2013**, *13*, 714–726.
3. Szakacs, G.; Paterson, J. K.; Ludwig, J. A.; Booth-Genthe, C.; Gottesman, M. M. Targeting Multidrug Resistance in Cancer. *Nat. Rev. Drug Discovery* **2006**, *5*, 219–234.
4. Bock, C.; Lengauer, T. Managing Drug Resistance in Cancer: Lessons from HIV Therapy. *Nat. Rev. Cancer* **2012**, *12*, 494–501.
5. Pasparakis, G.; Manouras, T.; Vamvakaki, M.; Argitis, P. Harnessing Photochemical Internalization with Dual Degradable Nanoparticles for Combinatorial Photo-Chemotherapy. *Nat. Commun.* **2014**, *5*, 3623.
6. Agostinis, P.; Berg, K.; Cengel, K. A.; Foster, T. H.; Girotti, A. W.; Gollnick, S. O.; Hahn, S. M.; Hamblin, M. R.; Juzeniene, A.; Kessel, D.; *et al.* Photodynamic Therapy of Cancer: An Update. *Ca-Cancer J. Clin.* **2011**, *61*, 250–281.
7. Celli, J. P.; Spring, B. Q.; Rizvi, I.; Evans, C. L.; Samkoe, K. S.; Verma, S.; Pogue, B. W.; Hasan, T. Imaging and Photodynamic Therapy: Mechanisms, Monitoring, and Optimization. *Chem. Rev.* **2010**, *110*, 2795–2838.
8. Lovell, J. F.; Liu, T. W. B.; Chen, J.; Zheng, G. Activatable Photosensitizers for Imaging and Therapy. *Chem. Rev.* **2010**, *110*, 2839–2857.
9. Cheng, Y.; Doane, T. L.; Chuang, C. H.; Ziady, A.; Burda, C. Near Infrared Light-Triggered Drug Generation and Release from Gold Nanoparticle Carriers for Photodynamic Therapy. *Small* **2014**, *10*, 1799–1804.
10. Master, A.; Livingston, M.; Sen Gupta, A. Photodynamic Nanomedicine in the Treatment of Solid Tumors: Perspectives and Challenges. *J. Controlled Release* **2013**, *168*, 88–102.
11. Dolmans, D. E. J. G. J.; Fukumura, D.; Jain, R. K. Photodynamic Therapy for Cancer. *Nat. Rev. Cancer* **2003**, *3*, 380–387.
12. Biel, M. Advances in Photodynamic Therapy for the Treatment of Head and Neck Cancers. *Laser Surg. Med.* **2006**, *38*, 349–355.
13. Mang, T. S.; Allison, R.; Hewson, G.; Snider, W.; Moskowitz, R. A Phase II/III Clinical Study of Tin Ethyl Etiopurpurin (Purlytin)-Induced Photodynamic Therapy for the Treatment of Recurrent Cutaneous Metastatic Breast Cancer. *Cancer J. Sci. Am.* **1998**, *4*, 378–384.
14. Ascencio, M.; Collinet, P.; Cosson, M.; Vinatier, D.; Mordon, S. The Place of Photodynamic Therapy in Gynecology. *Gynecol. Obstet. Fertil.* **2007**, *35*, 1155–1165.
15. Reddy, G. R.; Bhojani, M. S.; McConville, P.; Moody, J.; Moffat, B. A.; Hall, D. E.; Kim, G.; Koo, Y. E. L.; Woolliscroft, M. J.; Sugai, J. V.; *et al.* Vascular Targeted Nanoparticles for Imaging and Treatment of Brain Tumors. *Clin. Cancer Res.* **2006**, *12*, 6677–6686.
16. Barr, H.; Krasner, N.; Boulos, P. B.; Chatlani, P.; Bown, S. G. Photodynamic Therapy for Colorectal-Cancer—a Quantitative Pilot-Study. *Br. J. Surg.* **1990**, *77*, 93–96.
17. Ris, H. B.; Altermatt, H. J.; Inderbitzi, R.; Hess, R.; Nachbur, B.; Stewart, J. C. M.; Wang, Q.; Lim, C. K.; Bonnett, R.; Berenbaum, M. C.; *et al.* Photodynamic Therapy with Chlorins for Diffuse Malignant Mesothelioma—Initial Clinical-Results. *Br. J. Cancer* **1991**, *64*, 1116–1120.
18. Bown, S. G.; Rogowska, A. Z.; Whitelaw, D. E.; Lees, W. R.; Lovat, L. B.; Ripley, P.; Jones, L.; Wyld, P.; Gillams, A.; Hatfield, A. W. R. Photodynamic Therapy for Cancer of the Pancreas. *Gut* **2002**, *50*, 549–557.
19. Lou, P. J.; Jones, L.; Hopper, C. Clinical Outcomes of Photodynamic Therapy for Head-and-Neck Cancer. *Technol. Cancer Res. Treat.* **2003**, *2*, 311–317.
20. Bredell, M. G.; Besic, E.; Maake, C.; Walt, H. The Application and Challenges of Clinical PD-PDT in the Head and Neck Region A Short Review. *J. Photochem. Photobiol., B* **2010**, *101*, 185–190.
21. Ethirajan, M.; Chen, Y. H.; Joshi, P.; Pandey, R. K. The Role of Porphyrin Chemistry in Tumor Imaging and Photodynamic Therapy. *Chem. Soc. Rev.* **2011**, *40*, 340–362.
22. O'Connor, A. E.; Gallagher, W. M.; Byrne, A. T. Porphyrin and Nonporphyrin Photosensitizers in Oncology: Preclinical and Clinical Advances in Photodynamic Therapy. *Photochem. Photobiol.* **2009**, *85*, 1053–1074.
23. Davis, M. E.; Chen, Z.; Shin, D. M. Nanoparticle Therapeutics: an Emerging Treatment Modality for Cancer. *Nat. Rev. Drug Discovery* **2008**, *7*, 771–782.
24. Kim, C. S.; Duncan, B.; Creran, B.; Rotello, V. M. Triggered Nanoparticles as Therapeutics. *Nano Today* **2013**, *8*, 439–447.
25. Rosi, N. L.; Mirkin, C. A. Nanostructures in Biodiagnostics. *Chem. Rev.* **2005**, *105*, 1547–1562.
26. Li, S. D.; Huang, L. Pharmacokinetics and Biodistribution of Nanoparticles. *Mol. Pharmaceutics* **2008**, *5*, 496–504.
27. Kumar, R.; Roy, I.; Ohulchanskky, T. Y.; Vathy, L. A.; Bergey, E. J.; Sajjad, M.; Prasad, P. N. *In Vivo* Biodistribution and Clearance Studies Using Multimodal Organically Modified Silica Nanoparticles. *ACS Nano* **2010**, *4*, 699–708.
28. Nomoto, T.; Fukushima, S.; Kumagai, M.; Machitani, K.; Arnida; Matsumoto, Y.; Oba, M.; Miyata, K.; Osada, K.; *et al.* Three-Layered Polyplex Micelle as a Multifunctional Nanocarrier Platform for Light-Induced Systemic Gene Transfer. *Nat. Commun.* **2014**, *5*, 3545.
29. Zhen, Z.; Tang, W.; Chuang, Y. J.; Todd, T.; Zhang, W.; Lin, X.; Niu, G.; Liu, G.; Wang, L.; Pan, Z.; *et al.* Tumor Vasculature Targeted Photodynamic Therapy for Enhanced Delivery of Nanoparticles. *ACS Nano* **2014**, *8*, 6004–6013.
30. Cheng, L.; Wang, C.; Feng, L. Z.; Yang, K.; Liu, Z. Functional Nanomaterials for Phototherapies of Cancer. *Chem. Rev.* **2014**, *114*, 10869–10939.
31. Yavuz, M. S.; Cheng, Y.; Chen, J.; Cobley, C. M.; Zhang, Q.; Rycenga, M.; Xie, J.; Kim, C.; Song, K. H.; Schwartz, A. G.; *et al.* Gold Nanocages Covered by Smart Polymers for Controlled Release with Near-Infrared Light. *Nat. Mater.* **2009**, *8*, 935–939.
32. Liu, D.; Poon, C.; Lu, K.; He, C.; Lin, W. Self-Assembled Nanoscale Coordination Polymers with Trigger Release Properties for Effective Anticancer Therapy. *Nat. Commun.* **2014**, *5*, 4182.
33. He, C.; Lu, K.; Liu, D.; Lin, W. Nanoscale Metal-Organic Frameworks for the Co-Delivery of Cisplatin and Pooled siRNAs to Enhance Therapeutic Efficacy in Drug-Resistant Ovarian Cancer Cells. *J. Am. Chem. Soc.* **2014**, *136*, 5181–5184.
34. Huxford-Phillips, R. C.; Russell, S. R.; Liu, D.; Lin, W. Lipid-Coated Nanoscale Coordination Polymers for Targeted Cisplatin Delivery. *RSC Adv.* **2013**, *3*, 14438–14443.
35. Liu, D.; Kramer, S. A.; Huxford-Phillips, R. C.; Wang, S.; Della Rocca, J.; Lin, W. Coercing Bisphosphonates to Kill Cancer Cells with Nanoscale Coordination Polymers. *Chem. Commun.* **2012**, *48*, 2668–2670.
36. Huxford, R. C.; deKrafft, K. E.; Boyle, W. S.; Liu, D.; Lin, W. Lipid-Coated Nanoscale Coordination Polymers for Targeted Delivery of Antifolates to Cancer cells. *Chem. Sci.* **2012**, *3*, 198–204.
37. deKrafft, K. E.; Boyle, W. S.; Burk, L. M.; Zhou, O. Z.; Lin, W. Zr- and Hf-Based Nanoscale Metal-Organic Frameworks as Contrast Agents for Computed Tomography. *J. Mater. Chem.* **2012**, *22*, 18139–18144.

38. Liu, D.; Huxford, R. C.; Lin, W. Phosphorescent Nanoscale Coordination Polymers as Contrast Agents for Optical Imaging. *Angew. Chem., Int. Ed.* **2011**, *50*, 3696–3700.
39. deKrafft, K. E.; Burk, L. M.; Zhou, O. Z.; Lin, W. Nanoscale Coordination Polymers for CT Imaging. *Abstr. Pap. Am. Chem. Soc.* **2011**, 242.
40. Della Rocca, J.; Lin, W. Nanoscale Metal-Organic Frameworks: Magnetic Resonance Imaging Contrast Agents and Beyond. *Eur. J. Inorg. Chem.* **2010**, 3725–3734.
41. deKrafft, K. E.; Xie, Z.; Cao, G.; Tran, S.; Ma, L.; Zhou, O. Z.; Lin, W. Iodinated Nanoscale Coordination Polymers as Potential Contrast Agents for Computed Tomography. *Angew. Chem., Int. Ed.* **2009**, *48*, 9901–9904.
42. Taylor-Pashow, K. M. L.; Della Rocca, J.; Xie, Z.; Tran, S.; Lin, W. Postsynthetic Modifications of Iron-Carboxylate Nanoscale Metal-Organic Frameworks for Imaging and Drug Delivery. *J. Am. Chem. Soc.* **2009**, *131*, 14261–14262.
43. Rieter, W. J.; Pott, K. M.; Taylor, K. M. L.; Lin, W. Nanoscale Coordination Polymers for Platinum-Based Anticancer Drug Delivery. *J. Am. Chem. Soc.* **2008**, *130*, 11584–11585.
44. Jin, C. S.; Cui, L.; Wang, F.; Chen, J.; Zheng, G. Targeting-Triggered Porphysome Nanostructure Disruption for Activatable Photodynamic Therapy. *Adv. Healthcare Mater.* **2014**, *3*, 1240–1249.
45. Lovell, J. F.; Jin, C. S.; Huynh, E.; MacDonald, T. D.; Cao, W. G.; Zheng, G. Enzymatic Regioselection for the Synthesis and Biodegradation of Porphysome Nanovesicles. *Angew. Chem., Int. Ed.* **2012**, *51*, 2429–2433.
46. Lovell, J. F.; Jin, C. S.; Huynh, E.; Jin, H. L.; Kim, C.; Rubinstein, J. L.; Chan, W. C. W.; Cao, W. G.; Wang, L. V.; Zheng, G. Porphysome Nanovesicles Generated by Porphyrin Bilayers for Use as Multimodal Biophotonic Contrast Agents. *Nat. Mater.* **2011**, *10*, 324–332.
47. Carter, K. A.; Shao, S.; Hoopes, M. I.; Luo, D.; Ahsan, B.; Grigoryants, V. M.; Song, W. T.; Huang, H. Y.; Zhang, G. J.; Pandey, R. K.; *et al.* Porphyrin-Phospholipid Liposomes Permeabilized by Near-Infrared Light. *Nat. Commun.* **2014**, *5*, 3546.
48. Weis, R. M.; Mcconnell, H. M. Cholesterol Stabilizes the Crystal-Liquid Interface in Phospholipid Monolayers. *Biophys. J.* **1985**, *47*, A44–A44.
49. Alexis, F.; Pridgen, E.; Molnar, L. K.; Farokhzad, O. C. Factors Affecting the Clearance and Biodistribution of Polymeric Nanoparticles. *Mol. Pharmaceutics* **2008**, *5*, 505–515.
50. Dreher, M. R.; Liu, W. G.; Michelich, C. R.; Dewhirst, M. W.; Yuan, F.; Chilkoti, A. Tumor Vascular Permeability, Accumulation, and Penetration of Macromolecular Drug Carriers. *J. Natl. Cancer Inst.* **2006**, *98*, 335–344.
51. Khalil, I. A.; Kogure, K.; Akita, H.; Harashima, H. Uptake Pathways and Subsequent Intracellular Trafficking in Nonviral Gene Delivery. *Pharmacol. Rev.* **2006**, *58*, 32–45.
52. Siddik, Z. H. Cisplatin: Mode of Cytotoxic Action and Molecular Basis of Resistance. *Oncogene* **2003**, *22*, 7265–7279.
53. Castano, A. P.; Mroz, P.; Hamblin, M. R. Photodynamic Therapy and Anti-Tumour Immunity. *Nat. Rev. Cancer* **2006**, *6*, 535–545.
54. Jain, R. K.; Stylianopoulos, T. Delivering Nanomedicine to Solid Tumors. *Nat. Rev. Clin. Oncol.* **2010**, *7*, 653–664.
55. Igney, F. H.; Krammer, P. H. Death and Anti-Death: Tumour Resistance to Apoptosis. *Nat. Rev. Cancer* **2002**, *2*, 277–288.
56. Markman, J. L.; Rekechenetskiy, A.; Holler, E.; Ljubimova, J. Y. Nanomedicine Therapeutic Approaches to Overcome Cancer Drug Resistance. *Adv. Drug Delivery Rev.* **2013**, *65*, 1866–1879.
57. Kirtane, A. R.; Kalscheuer, S. M.; Panyam, J. Exploiting Nanotechnology to Overcome Tumor Drug Resistance: Challenges and Opportunities. *Adv. Drug Delivery Rev.* **2013**, *65*, 1731–1747.
58. Della Rocca, J.; Liu, D.; Lin, W. Nanoscale Metal-Organic Frameworks for Biomedical Imaging and Drug Delivery. *Acc. Chem. Res.* **2011**, *44*, 957–968.
59. Peer, D.; Karp, J. M.; Hong, S.; FarokHzad, O. C.; Margalit, R.; Langer, R. Nanocarriers as an Emerging Platform for Cancer Therapy. *Nat. Nanotechnol* **2007**, *2*, 751–760.
60. Lehar, J.; Krueger, A. S.; Avery, W.; Heilbut, A. M.; Johansen, L. M.; Price, E. R.; Rickles, R. J.; Short, G. F.; Staunton, J. E.; Jin, X. W.; *et al.* Synergistic Drug Combinations Tend to Improve Therapeutically Relevant Selectivity. *Nat. Biotechnol.* **2009**, *27*, 864–864.
61. Henderson, B. W.; Donovan, J. M. Release of Prostaglandin E2 from Cells by Photodynamic Treatment *In Vitro*. *Cancer Res.* **1989**, *49*, 6896–900.
62. Henderson, B. W.; Owczarczak, B.; Sweeney, J.; Gessner, T. Effects of Photodynamic Treatment of Platelets or Endothelial Cells *In Vitro* on Platelet Aggregation. *Photochem. Photobiol.* **1992**, *56*, 513–521.
63. Torchilin, V. Tumor Delivery of Macromolecular Drugs Based on the EPR Effect. *Adv. Drug Delivery Rev.* **2011**, *63*, 131–135.
64. Bellnier, D. A.; Greco, W. R.; Loewen, G. M.; Nava, H.; Oseroff, A. R.; Dougherty, T. J. Clinical Pharmacokinetics of the PDT Photosensitizers Porfimer Sodium (Photofrin), 2-[1-hexyloxyethyl]-2-Devinyl Pyropheophorbide-a (Photochlor) and 5-ALA-Induced Protoporphyrin IX. *Laser Surg. Med.* **2006**, *38*, 439–444.
65. Dunn, J. M.; Mackenzie, G. D.; Banks, M. R.; Mosse, C. A.; Haidry, R.; Green, S.; Thorpe, S.; Rodriguez-Justo, M.; Winstanley, A.; Novelli, M. R.; *et al.* Randomised Controlled Trial of ALA *vs*. Photofrin Photodynamic Therapy for High-Grade Dysplasia Arising in Barrett's Oesophagus. *Laser Med. Sci.* **2013**, *28*, 707–715.
66. Hunt, D. W. C.; Sorrenti, R. A.; Renke, M. E.; Waterfield, E.; Levy, J. G. Accelerated Myelopoietic Recovery in Irradiated Mice Treated with Photofrin(R). *Int. J. Immunopharmacol.* **1995**, *17*, 33–39.
67. Jiang, F.; Lilge, L.; Logie, B.; Li, Y.; Chopp, M. Photodynamic Therapy of 9L Gliosarcoma with Liposome-Delivered Photofrin. *Photochem. Photobiol.* **1997**, *65*, 701–706.
68. Nishiyama, N.; Okazaki, S.; Cabral, H.; Miyamoto, M.; Kato, Y.; Sugiyama, Y.; Nishio, K.; Matsumura, Y.; Kataoka, K. Novel Cisplatin-Incorporated Polymeric Micelles can Eradicate Solid Tumors in Mice. *Cancer Res.* **2003**, *63*, 8977–8983.
69. Lin, J.; Wang, S. J.; Huang, P.; Wang, Z.; Chen, S. H.; Niu, G.; Li, W. W.; He, J.; Cui, D. X.; Lu, G. M.; *et al.* Photosensitizer-Loaded Gold Vesicles with Strong Plasmonic Coupling Effect for Imaging-Guided Photothermal/Photodynamic Therapy. *ACS Nano* **2013**, *7*, 5320–5329.